6

Diffraction by perfect crystals

The X-ray beam from a synchrotron source is polychromatic. Typical values for the bandwidth in energy vary between a fraction of a keV for an undulator, up to a few hundred keV or so in the case of a bending magnet. Many experiments require a monochromatic beam, where both the energy and energy bandwidth can be set to convenient values. By far the most common type of monochromator is a crystal that Bragg reflects an energy band, or equivalently wavelength band, out of the incident beam. The band is centred around a wavelength λ given by Bragg's Law, $m\lambda = 2d \sin\theta$, where d is the lattice spacing, θ is the angle between the incident beam and the lattice planes, and m is a positive integer.

One requirement of a monochromator crystal is that it preserves the inherently good angular collimation of the synchrotron beam, which is of order 0.1 mrad. For this reason, perfect crystals, which are essentially free from any defects or dislocations, are often used. However, even a perfect crystal does not have an infinitely sharp response, but instead has an intrinsic width. This width may be defined in various ways, depending on the type of experiment imagined. Here we shall start out by considering the relative wavelength band, $\zeta = (\Delta\lambda/\lambda)$, a perfect crystal reflects out of a white, parallel incident beam.

Candidate monochromator crystals must not only be perfect, but they should maintain their perfection when subjected to the large heat loads imposed by the incident white beam. In practice, few materials can meet these exacting requirements. Most monochromators are either fabricated from silicon, diamond or germanium, with each having its own advantages depending on the application, as discussed later.

To develop a theory of the diffraction of X-rays from perfect crystals it is necessary to go beyond the kinematical approximation used in Chapter 5. This approximation applies to imperfect crystals, formed from microscopic mosaic blocks (see Fig. 5.19 on page 183). The size of these blocks is taken to be small, in the sense that the magnitude of the X-ray wavefield does not change appreciably over the depth of the block[1]. The scattering amplitude is then evaluated by summing together the amplitude of the waves scattered by each unit cell, taking into account the appropriate phase factors. Diffraction from macroscopic perfect crystals is fundamentally different from this scenario. As the incident wave propagates down into the crystal its amplitude diminishes, as a small fraction is reflected into the exit

Elements of Modern X-ray Physics, Second Edition Jens Als-Nielsen and Des McMorrow

[1] The X-ray beam may of course be attenuated by absorption.

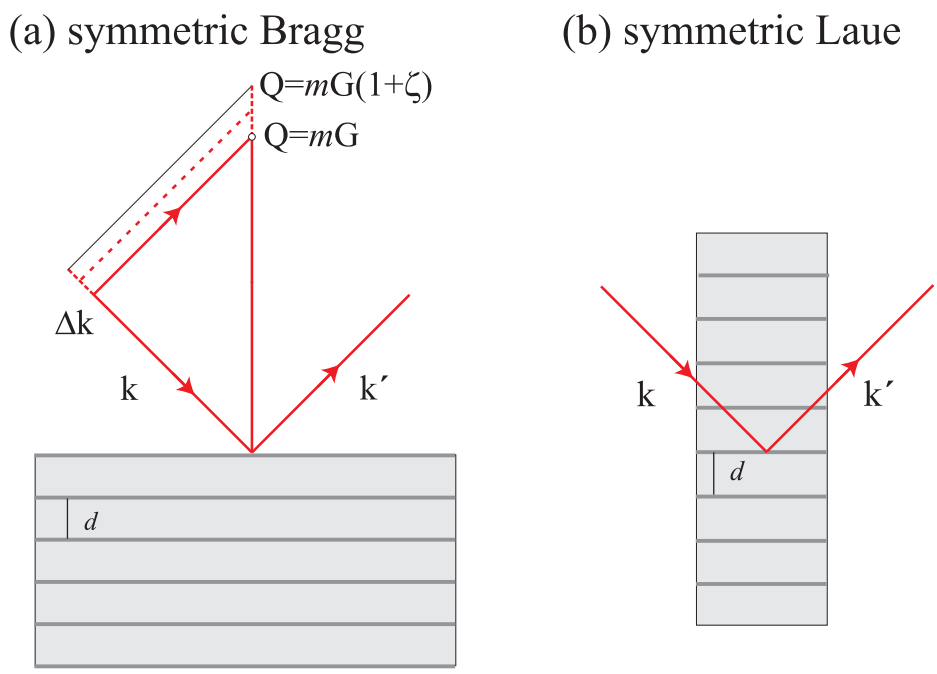

Fig. 6.1 Diffraction by a crystal with a lattice spacing of d in (a) Bragg reflection and (b) Laue transmission geometries. Both cases are symmetric since the incident and exit beams form the same angle with respect to the physical surface. The incident beam is assumed to be parallel and white. The crystal reflects a width in wavevector given by Δk. The small variable ζ is defined by $\zeta = \Delta G/G \equiv \Delta k/k$. The relative energy bandwidth or wavelength bandwidth is also equal to $\Delta k/k$.

beam as it passes through each atomic plane. In addition there is a chance that the reflected beam will be re-scattered into the direction of the incident beam before it has left the crystal. The theory which has been developed to allow for these multiple scattering effects is known as dynamical diffraction theory.

At the outset it is important to specify exactly the scattering geometry, as it transpires that this has a profound influence on the diffraction profile from a perfect crystal. Diffraction may occur either in reflection or transmission, which are known as Bragg and Laue geometries respectively, as shown in Fig. 6.1. The angle that the physical surface makes with respect to the reflecting atomic planes is also an important factor. The reflection is said to be symmetric if the surface normal is perpendicular (parallel) to the reflecting planes in the case of Bragg (Laue) geometry. Otherwise it is asymmetric. Within the kinematical approximation the scattering is independent of the geometry. To take one striking example of how the diffraction profile from a perfect crystal is affected by the geometry, consider the symmetric Bragg and Laue cases (Fig. 6.1), and imagine that the incident beam is perfectly collimated and white, in the sense that it contains a continuous distribution of wavelengths. As we shall see, in the Bragg case the collimation of the beam is preserved, whereas the Laue geometry imparts an angular divergence to the reflected beam even though the incident beam is perfectly collimated. To start with we shall examine the symmetric Bragg case, and later explain how the results are modified with the crystal set in an asymmetric Bragg or Laue geometry.

The approach followed here is essentially the same as the one first developed by C. G. Darwin in 1914. In his method, Darwin treated the crystal as an infinite stack of atomic planes, each of which gives rise to a weak reflected wave which may subsequently be re-scattered into the direction of the

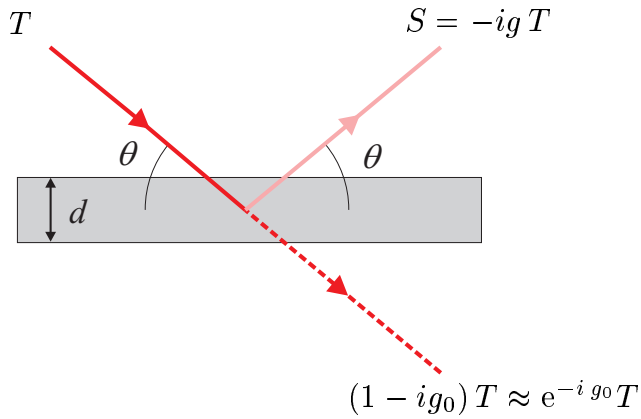

Fig. 6.2 A wave T incident on a sheet of unit cells will be partly reflected and partly transmitted. The reflected wave is $-i\,gT$, and the transmitted wave is $T(1 - ig_0)$, where g and g_0 are small parameters given in the text.

incident beam. An alternative approach was developed by Ewald (1916-1917), and later re-formulated by von Laue (1931). They treated the crystal as a medium with a periodic dielectric constant, and then solved Maxwell's equations to obtain results in agreement with those derived earlier by Darwin.

Before deriving the dynamical theory, the reader is reminded of a few important results concerning the reflectivity from a thin slab. The kinematical diffraction from a stack of thin slabs is then calculated. This differs from the discussion in Chapter 5 as effects due to refraction are now included. The kinematical approximation is of importance, as any dynamical theory must give the same results in the limit of weak scattering.

6.1 One atomic layer: reflection and transmission

Consider an X-ray beam incident on a thin layer of electrons of density ρ and with a thickness d, such that $d \ll \lambda$, as shown in Fig. 6.2. The incident wave, T, is partly reflected specularly from the layer, and partly transmitted through it. From Eq. (3.24) in Chapter 3 we know that the reflected wave is phase shifted by $-\frac{\pi}{2}$ (*i.e.* by a factor of $-i$) with respect to the incident wave, and has an amplitude equal to

$$g = \frac{\lambda r_0 \rho\, d}{\sin\theta}$$

To generalise this expression so that it is applicable to the scattering from a layer of unit cells, the density ρ is replaced by $|F|/v_c$, where F is the structure factor of the unit cell, and v_c is its volume. This is a necessary step, as it can no longer be assumed that d is small compared to the wavelength, and hence destructive interference will reduce the scattering at higher scattering angles (see Section 4.2). Using Bragg's law, $m\lambda = 2d\sin\theta$ the above becomes

$$g = \frac{[2d\sin\theta/m]\, r_0\, (|F|/v_c)\, d}{\sin\theta} = \frac{1}{m}\left(\frac{2d^2 r_0}{v_c}\right)|F| \tag{6.1}$$

Since v_c is of order d^3, g is of order $r_0/d \simeq 10^{-5}$, and the reflectivity of even a thousand layers is approximately 10^{-2} only[2]. For simplicity the incident wave has been assumed to be polarized with its electric field perpendicular to the plane containing the wavevectors of the incident and reflected beams, so that the polarization factor, P, is unity (see Eq. (1.8)).

The transmitted wave in Fig. 6.2 may be written as $(1 - ig_0)T \approx \mathrm{e}^{-ig_0}T$, since g_0 is the small real number given by Eq. (3.6) on page 75. This equation may be recast in terms of g as

$$g_0 = \frac{|F_0|}{|F|}\, g \tag{6.2}$$

Here F_0 is the unit-cell structure factor in the forward direction, *i.e.* $\mathrm{Q} = \theta = 0$. We note that for forward scattering the polarization factor is always equal to unity, independent of the polarization of the incident beam.

6.2 Kinematical reflection from a few layers

A single layer of atoms reflects an X-ray beam only very weakly. It is straightforward to derive the reflectivity from a stack of N layers as long as the product of N and the reflectivity per layer, g, is small, *i.e.* $Ng \ll 1$. In this case we simply add the amplitude of rays reflected from layers at different depths in the stack, taking into account the phase factor $\mathrm{e}^{i\mathrm{Q}dj}$, where j labels the layer. This is the so-called kinematical approximation, and the *amplitude* reflectivity for N layers is

$$\begin{aligned} r_N(\mathrm{Q}) &= -ig \sum_{j=0}^{N-1} \mathrm{e}^{i\mathrm{Q}dj}\mathrm{e}^{-ig_0 j}\mathrm{e}^{-ig_0 j} \\ &= -ig \sum_{j=0}^{N-1} \mathrm{e}^{i(\mathrm{Q}d-2g_0)j} \end{aligned} \tag{6.3}$$

The phase shift is $2g_0$ rather than just g_0 as each layer is traversed twice, once in the T direction, and once in the S direction.

The reciprocal lattice of a stack of layers with layer spacing d is a line of points in reciprocal space at multiples, m, of $\mathrm{G} = 2\pi/d$. In general we are interested in small, relative deviations of the scattering vector Q away from mG, so that

$$\mathrm{Q} = m\mathrm{G}\,(1 + \zeta) \tag{6.4}$$

where ζ is then the small relative deviation (see Fig. 6.1). This is equivalent to the relative bandwidth in energy (or wavelength) since

$$\zeta = \frac{\Delta\mathrm{Q}}{\mathrm{Q}} = \frac{\Delta\mathrm{k}}{\mathrm{k}} = \frac{\Delta\mathcal{E}}{\mathcal{E}} = \frac{\Delta\lambda}{\lambda} \tag{6.5}$$

[2]Writing Bragg's law as $m\lambda = 2d\sin\theta$ implies that d is the longest lattice spacing for a given family of planes (h, k, l). For example, if one is considering the (220) reflection, say, then the d spacing is calculated for the (110) planes, and the appropriate value of m is 2.

The phase appearing in the exponential of Eq. (6.3) can thus be re-written in terms of ζ as

$$\begin{aligned} \mathrm{Q}d - 2g_0 &= m\mathrm{G}(1+\zeta)\,\frac{2\pi}{\mathrm{G}} - 2g_0 \\ &= 2\pi\left(m + m\zeta - \frac{g_0}{\pi}\right) \end{aligned}$$

The sum then becomes

$$\begin{aligned} \sum_{j=0}^{N-1} \mathrm{e}^{i\,(\mathrm{Q}d-2g_0)j} &= \sum_{j=0}^{N-1} \mathrm{e}^{i\,2\pi m j}\mathrm{e}^{i\,2\pi(m\zeta-g_0/\pi)j} \\ &= \sum_{j=0}^{N-1} \mathrm{e}^{i\,2\pi(m\zeta-g_0/\pi)j} \end{aligned}$$

and this geometric series can be summed (see page 52) to yield

$$|r_N(\zeta)| = g\left|\frac{\sin(\pi N[m\zeta-\zeta_0])}{\sin(\pi[m\zeta-\zeta_0])}\right| \tag{6.6}$$

where ζ_0 is the displacement of the Bragg peak defined by

$$\boxed{\zeta_0 = \frac{g_0}{\pi} = \frac{2d^2|F_0|}{\pi m v_c}\,r_0} \tag{6.7}$$

To derive the explicit expression for ζ_0 above we have used the defining expression for g_0 in Eq. (3.6) with $\Delta = d$, $\sin\theta = m\lambda/(2d)$ and $\rho_a f^0(0) = |F_0|/v_c$.

From Eq. (6.6) the maximum amplitude reflectivity is Ng, and occurs when $\zeta = \zeta_0/m$. Therefore the reflectivity does not have its maximum at the reciprocal lattice points, but is displaced by a *relative* amount ζ_0/m. It follows from Eq. (6.4) that the *absolute* displacement is $m\mathrm{G}(\zeta_0/m) = \mathrm{G}\zeta_0$ which according to Eq. (6.7) varies as $1/m$. This displacement arises from the refraction of the incident wave as it enters the crystal, an effect that is usually neglected in the derivation of Bragg's law. The index of refraction is less than unity for X-rays, and inside the crystal the modulus of the X-ray wavevector has a smaller value than outside. For a fixed incident angle, the value of k outside of the crystal must be larger than $m\mathrm{G}/(2\sin\theta)$ in order to obtain maximal constructive interference, *i.e.* $\zeta_0 > 0$ as is also clear from Eq. (6.7).

For the kinematical approximation to be valid it is required that $Ng \ll 1$. Adding more and more layers with a reflectivity g per layer increases the peak reflectivity, but of course it can never exceed 100%. Close to $\zeta = \zeta_0/m$ the line shape starts to deviate from $|r_N(\zeta)|^2$ given by Eq. (6.6), and we enter into the dynamical diffraction as indicated by the shading in Fig. 6.3. However, when far enough away from the Bragg condition, *i.e.* when ζ is sufficiently different from ζ_0/m, the kinematical approximation is still valid, even for many layers. When N becomes large the side lobes of the function $|r_N(\zeta)|^2$ become closely spaced, and the rapidly varying numerator $\sin^2(N\pi[m\zeta-\zeta_0])$ can be approximated by its average value of 1/2 to obtain

$$|r_N(\zeta)|^2 \to \frac{g^2}{2\sin^2(\pi[m\zeta-\zeta_0])} \approxeq \frac{g^2}{2(\pi[m\zeta-\zeta_0])^2} \tag{6.8}$$

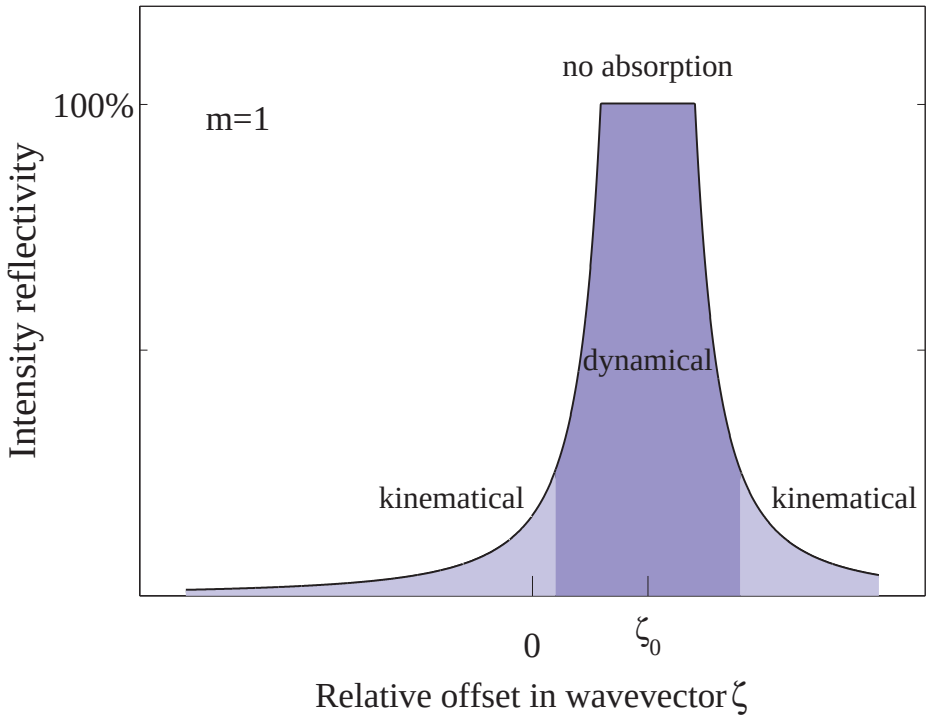

Fig. 6.3 The intensity reflectivity from a stack of N atomic layers. The relative deviation from the Bragg condition is given by the parameter ζ. The reflectivity is peaked not at $\zeta = 0$, but at $\zeta_0 = g_0/(m\pi)$ due to refraction of the X-ray beam inside of the crystal. When $|\zeta - \zeta_0|$ is large the reflectivity is small, and we are in the kinematical regime as indicated by the lighter shading. As $|\zeta - \zeta_0| \to 0$ the kinematical approximation breaks down, and the reflectivity is then described by dynamical theory.

The significance of this result is that a correct dynamical diffraction theory must attain this limiting form for large values of $|\zeta - \zeta_0|$. In Fig. 6.3 the kinematical region is indicated by the lighter shading.

Dynamical reflection takes place near a reciprocal lattice point, and must join the kinematic reflection regime in a continuous way. It has been shown in Section 5.3 that the surface gives rise to rods of scattering in a direction perpendicular to the physical surface. Continuity then requires that the region of dynamical diffraction and these so-called crystal truncations rods must be connected in a continuous manner. This has the somewhat surprising consequence that the reflection from an asymmetric cut crystal is no longer specular – specular reflection only occurs from a symmetrically cut crystal in Bragg geometry. We shall return to this issue at the end of this chapter.

6.3 Darwin theory and dynamical diffraction

We now turn our attention to the problem of how to calculate the scattering from an infinite stack of atomic planes, where each one reflects and transmits the incident wave according to the equations given in Section 6.1. The planes are labelled by the index j, with the surface plane defined by $j = 0$ (Fig. 6.4(a)). The objective is to calculate the amplitude reflectivity, which is the ratio of the total reflected wavefield S_0 to that of the incident field T_0.

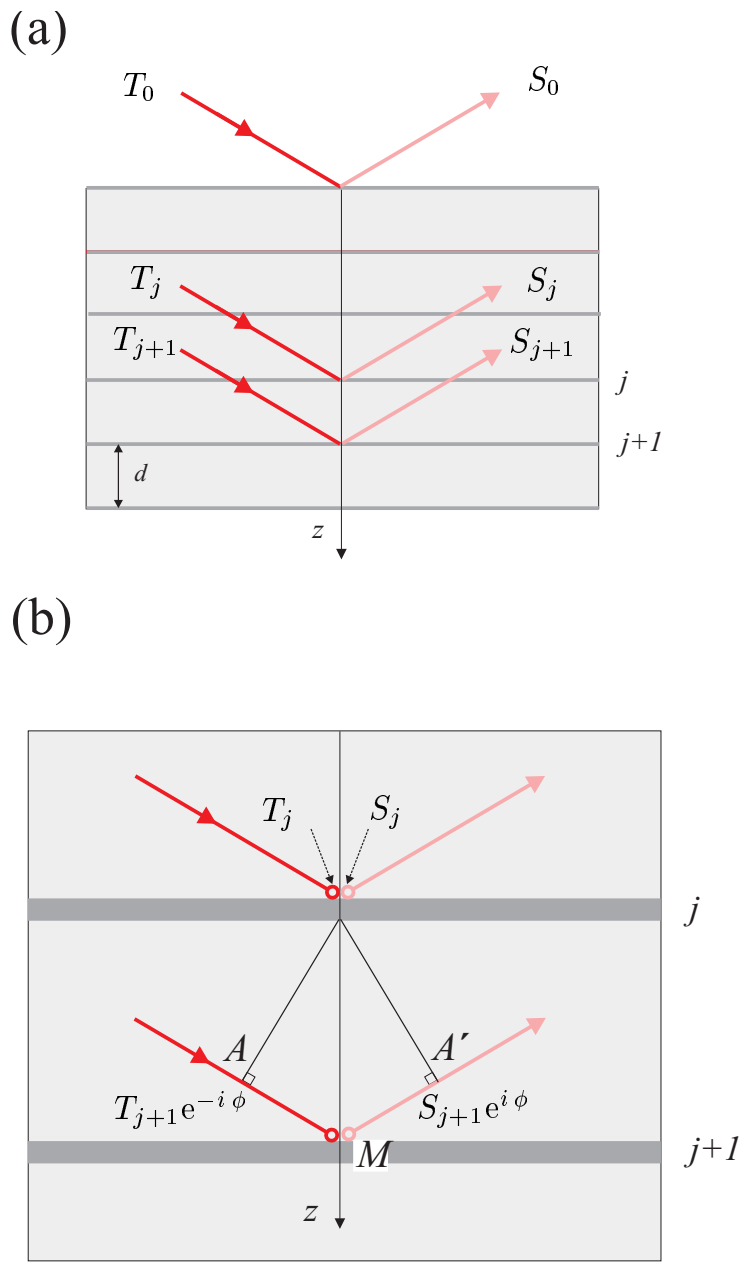

Fig. 6.4 Definition of the T and S wavefields. (a) The amplitude reflectivity is given by S_0/T_0. (b) Schematic used to derive the difference equations. The S field at A' is related to the S field just above the atomic plane at M by the phase factor $e^{i\phi}$. The field $S_{j+1}e^{i\phi}$ is then the same as the S_j field just below layer j. Above layer j it gets an extra contribution $(-igT_j)$, from reflection of the T field. Similar arguments apply to the T field.

Both outside and within the crystal there are two wavefields: the T field propagating in the direction of the incident beam, and the S field in the direction of the reflected beam. These fields change abruptly when they pass through the atomic planes for two reasons. First, a small fraction, equal to $-ig$, of the wave is reflected. Second, the transmitted wave is phase shifted by an amount $(1 - ig_0)$. The derivation of Bragg's law relies on the fact that the reflected wave from layer $j + 1$ is in phase with the one from layer j if the pathlength differs by an integer number of wavelengths. In Fig. 6.4(b) this corresponds to the requirement[3] that the distance AMA' is equal to $m\lambda$, or equivalently that the phase shift in going from A to M is $m\pi$. As we are interested in deriving the (small) bandwidth of the reflecting region, the phase is restricted to small deviations about $m\pi$, and the phase is then given by

$$\phi = m\pi + \Delta$$

where Δ is a small parameter. The relative deviation in phase is therefore $\Delta/(m\pi)$, which must be equal to the corresponding relative deviation in scattering vector, ζ (Eq. (6.4)), so that

$$\Delta = m\pi\,\zeta \tag{6.9}$$

In our development of Darwin's theory Δ will be used as the independent variable. We remind the reader that we are considering a perfectly collimated incident beam, so that the variation of Δ is through the variation of incident energy (or wavenumber), *c.f.* Eq. (6.5). Later when the algebra has been worked through, the results will be recast in terms of ζ, which is more useful for comparisons with experiment.

The fundamental difference equations

Let the T field just *above* layer j on the z axis be denoted T_j, and similarly for S_j. The S field just above layer $j + 1$ is S_{j+1} on the z axis, that is the point M in Fig. 6.4. At point A' it is $S_{j+1}e^{i\phi}$, and indeed it must have this value at any point on the wavefront through A', including the point on the z axis just below the j'th plane. On being transmitted through the j'th layer it changes its phase by the small amount $-ig_0$ so that the S field just above the j'th layer, which by definition is S_j, can be written as $(1 - ig_0)S_{j+1}e^{i\phi}$. To obtain the total field, we must also add the part due to the reflection of the wave T_j. In total then we have

$$S_j = -ig\,T_j + (1 - ig_0)S_{j+1}e^{i\phi} \tag{6.10}$$

Next consider the T field just below the j'th layer. This must be the same field that exits at M, except that its phase is shifted by an amount that corresponds to the distance from M to A, *i.e.* $T_{j+1}e^{-i\phi}$. This field is composed of contributions from the field T_j after it has been transmitted through the j'th layer, and from the wave $S_{j+1}e^{i\phi}$ after it has been reflected from the bottom of the j'th layer. This leads to the second difference equation

$$T_{j+1}e^{-i\phi} = (1 - ig_0)T_j - ig\,S_{j+1}e^{i\phi} \tag{6.11}$$

The coupled T to S fields in Eq. (6.11) and (6.10) are separated in the following way.

[3] Here it should be understood that λ is the wavelength inside the crystal, not the wavelength of the incident beam outside of the crystal.

Separating the T and S fields

We rewrite Eq. (6.11) as

$$ig\,S_{j+1} = (1 - ig_0)T_j e^{-i\phi} - T_{j+1}e^{-i\,2\phi} \tag{6.12}$$

The validity of this equation does not depend on the labelling, and in particular it must also hold for the field S_j. Replacing $j+1$ by j, and j by $j-1$ yields

$$ig\,S_j = (1 - ig_0)T_{j-1}e^{-i\phi} - T_j e^{-i\,2\phi} \tag{6.13}$$

The expressions for $ig\,S_{j+1}$ and $ig\,S_j$ given in Eq. (6.12) and (6.13) can now be substituted into Eq. (6.10) (after multiplying it by a factor of ig) to obtain an equation purely in terms of the T fields:

$$(1 - ig_0)T_{j-1}e^{-i\phi} - T_j\,e^{-i\,2\phi} = g^2\,T_j + (1 - ig_0)[(1 - ig_0)T_j - T_{j+1}e^{-i\phi}]$$

Collecting the coefficients of T_{j+1}, T_j and T_{j-1} together one finds

$$(1 - ig_0)e^{-i\phi}[T_{j+1} + T_{j-1}] = [g^2 + (1 - ig_0)^2 + e^{-i\,2\phi}]T_j \tag{6.14}$$

Trial solution for the T and S fields

Possible solutions to the equation for the T fields are now considered. The fields T_j and T_{j+1} are almost out of phase, as is apparent from Eq. (6.11), since ϕ is approximately $m\pi$ and g_0 and g are small parameters. Moreover, it is expected that the T field is attenuated as it penetrates into the crystal, since a fraction of the incident beam is reflected out of the crystal when it passes through each atomic plane. A suitable trial solution therefore has the form

$$T_{j+1} = e^{-\eta}e^{i\,m\pi}\,T_j \tag{6.15}$$

where η is in general complex. In order that the beam is attenuated only slightly from one plane to the next the real part of η must be small and positive. Inserting our trial solution into Eq. (6.14), and noting that $e^{-i\,\phi} = e^{-i\,m\pi}e^{-i\,\Delta}$ and that $e^{\pm i\,2m\pi} = 1$ yields

$$(1 - ig_0)e^{-i\,\Delta}[e^{-\eta} + e^{\eta}] = g^2 + (1 - ig_0)^2 + e^{-i\,2\Delta}$$

Use is now made of the fact that all of the parameters in the above expression are small compared to unity. By expansion one finds cancellation of zero and first-order terms on the left and right hand sides. Equating second-order terms leads to the expression for η:

$$\eta^2 = g^2 - (\Delta - g_0)^2$$

which has the solution

$$\boxed{i\,\eta = \pm\sqrt{(\Delta - g_0)^2 - g^2}} \tag{6.16}$$

For the S fields the trial solution reads

$$S_{j+1} = e^{-\eta}e^{i\,m\pi}\,S_j$$

and it can be shown that it yields the same equation for η.

Amplitude reflectivity, S_0/T_0

We are now in a position to calculate the amplitude reflectivity r, *i.e.* the ratio of S_0/T_0. First we set $j = 0$ in the above, and obtain $S_1 = \mathrm{e}^{-\eta}\mathrm{e}^{i m\pi} S_0$. This is inserted into Eq. (6.10), also with $j = 0$, to give

$$S_0 = -ig\, T_0 + (1 - ig_0) S_0 \mathrm{e}^{-\eta}\mathrm{e}^{i m\pi}\mathrm{e}^{i m\pi}\mathrm{e}^{i\Delta} \tag{6.17}$$

This is then rearranged to read

$$\begin{aligned}\frac{S_0}{T_0} &\approxeq \frac{-i\, g}{1 - (1 - i\, g_0)(1 - \eta)(1 + i\Delta)} \\ &\approxeq \frac{-i\, g}{i g_0 + \eta - i\,\Delta} = \frac{g}{i\eta + (\Delta - g_0)}\end{aligned}$$

Defining for convenience a new variable ϵ by

$$\epsilon = \Delta - g_0 = m\pi\zeta - \pi\zeta_0$$

and inserting the solution for $i\eta$ into the expression for S_0/T_0 leads to

$$\boxed{r = \frac{S_0}{T_0} = \frac{g}{i\eta + \epsilon} = \frac{g}{\epsilon \pm \sqrt{\epsilon^2 - g^2}}} \tag{6.18}$$

This completes our derivation of the Darwin reflectivity curve. There is, however, one point left to clarify, and that is the possible ambiguity over which sign to take with the square root in the above. To resolve this we note that if we choose the positive sign for ϵ positive, then in the limit of $\epsilon \gg g$ the intensity reflectivity decreases as $(g/(2\epsilon))^2$. For negative ϵ we choose the negative sign, as with this choice for $|\epsilon| \gg g$ the intensity reflectivity will again decrease as $(g/(2\epsilon))^2$. For $|\epsilon| < g$ the square root is purely imaginary, and the intensity reflectivity, evaluated as S_0/T_0 multiplied by its complex conjugate, is unity. This is the region of *total* reflection. In Fig. 6.5 we plot the intensity reflectivity as a function of ϵ/g. The many interesting aspects of this curve are discussed in the following section.

6.4 The Darwin reflectivity curve

In order to obtain explicit formulae for the Darwin reflectivity curve the variable x is introduced and defined by

$$x = \frac{\epsilon}{g}$$

This is related to the variable ζ through

$$x = \frac{\epsilon}{g} = \frac{\Delta - g_0}{g} = m\pi\frac{\zeta}{g} - \frac{g_0}{g} \tag{6.19}$$

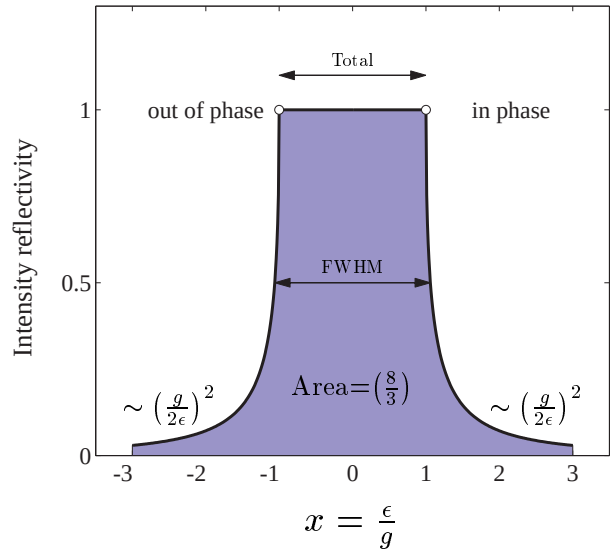

Fig. 6.5 The Darwin reflectivity curve calculated from Eq. (6.21). For values of x between -1 and 1 the reflectivity is 100%. This is known as the region of total reflection. For large values of $|x|$ the intensity decays as $1/(2x)^2$. At $x = 1$ the the X-ray wavefield has its maxima on the atomic planes, whereas for $x = -1$ the nodes of the wavefield coincide with the atomic planes.

where m is the order of the reflection, *i.e.* $m = 1$ is the fundamental, $m = 2$ is the second-order, etc. From Eq. (6.18) the amplitude reflectivity curve in terms of x is

$$r(x) = \left(\frac{S_0}{T_0}\right) = \begin{cases} \dfrac{1}{x + \sqrt{x^2 - 1}} = x - \sqrt{x^2 - 1} & \text{for } x \geq 1 \\ \dfrac{1}{x + i\sqrt{1 - x^2}} = x - i\sqrt{1 - x^2} & \text{for } |x| \leq 1 \\ \dfrac{1}{x - \sqrt{x^2 - 1}} = x + \sqrt{x^2 - 1} & \text{for } x \leq -1 \end{cases} \tag{6.20}$$

It follows that the intensity reflectivity is

$$R(x) = \left(\frac{S_0}{T_0}\right)\left(\frac{S_0}{T_0}\right)^* = \begin{cases} \left(x - \sqrt{x^2 - 1}\right)^2 & \text{for } x \geq 1 \\ 1 & \text{for } |x| \leq 1 \\ \left(x + \sqrt{x^2 - 1}\right)^2 & \text{for } x \leq -1 \end{cases} \tag{6.21}$$

which is plotted in Fig. 6.5. A key feature of the Darwin reflectivity curve is that the phase shift between the T_0 and S_0 fields varies across it. This is illustrated in Fig. 6.6 where we plot the phase of the amplitude reflectivity r as a function of x. The two fields are exactly out of phase by $-\pi$ (or equivalently π) for $x \leq -1$, and in phase for $x \geq 1$.

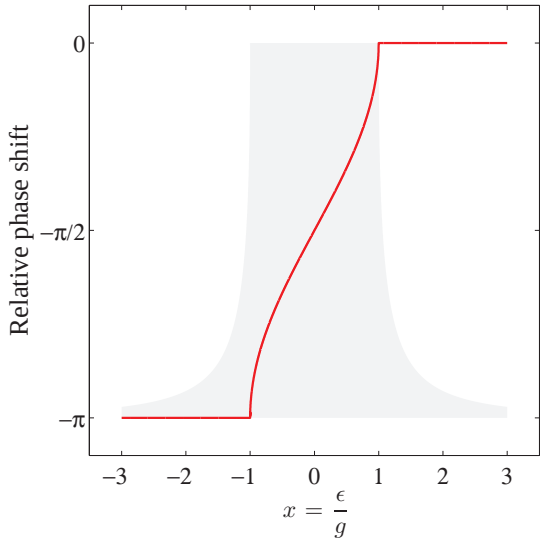

Fig. 6.6 The relative phase shift between the incident T_0 and reflected S_0 wavefields as calculated from Eq. (6.20). For reference, the Darwin curve is shown in shaded relief in the background. The two wavefileds are out of phase, here chosen to be $-\pi$, for $x \leq -1$, and in phase for $x \geq 1$.

The asymptotic form of $R(x)$ for $x \gg 1$ is

$$R(x) = \left(\sqrt{x^2(1 - \frac{1}{x^2})} - x \right)^2 \cong \left(x(1 - \frac{1}{2x^2}) - x \right)^2$$
$$= \frac{1}{4x^2} \qquad \text{for} \quad x \gg 1 \tag{6.22}$$

This should be compared to the expected asymptotic form for the kinematical region, discussed in Section 6.2. In terms of the variable x, Eq. (6.8) reads

$$|r_N(\zeta)|^2 \to \frac{1}{2x^2} \quad \text{for} \quad x \gg 1 \tag{6.23}$$

i.e. twice the result given by dynamical theory. The reason for this is subtle. In Section 6.2 the equations were derived on the assumption that the scattering arises from a finite stack of layers: the top and the bottom of the stack. Hence the wave encounters *two* interfaces. By contrast, Darwin's formalism assumes an infinite stack of layers, with only a single interface, the surface. The two asymptotic forms are therefore consistent.

6.4.1 Darwin width

One of the key parameters we are interested in obtaining is a measure of the width of the Darwin reflectivity curve. From Fig. 6.5 it is clear that there are several alternatives. First of all there is the region ($|x| < 1$) of total reflection itself, which has a width in x of 2. The relationship between x and the variable ζ is given in Eq. (6.19). This is rearranged to read

$$\zeta = \frac{gx + g_0}{m\pi} \tag{6.24}$$

	$\zeta_D^{FWHM} \times 10^6$								
	(111)			(220)			(400)		
Diamond	61.0			20.9			8.5		
a= 3.5670 Å	3.03	0.018	-0.01	1.96	0.018	-0.01	1.59	0.018	-0.01
Silicon	139.8			61.1			26.3		
a= 5.4309 Å	10.54	0.25	-0.33	8.72	0.25	-0.33	7.51	0.25	-0.33
Germanium	347.2			160.0			68.8		
a= 5.6578 Å	27.36	-1.1	-0.89	23.79	-1.1	-0.89	20.46	-1.1	-0.89

Table 6.1 The calculated Darwin widths for the (111), (220) and (400) reflections in symmetric Bragg geometry from diamond, silicon, and germanium. For each reflection the values of f^0(Q), f', f'' have also been listed. The values of f^0(Q) have been calculated from the coefficients given in Table 4.1, and the values of f' and f'' are for a wavelength of 1.5405 Å, and have been taken from The International Tables of Crystallography. Here it has been assumed that the incident beam is polarized perpendicular to the scattering plane ($\hat{\sigma}$ polarization). For $\hat{\pi}$ polarization the widths have to be multiplied by a factor of $\cos(2\theta)$.

so that a width in x of 2 translates into a width in ζ of $2g/(m\pi)$. Thus the width ζ_D^{total} of the region of total reflectivity is

$$\boxed{\zeta_D^{\text{total}} = \frac{2g}{m\pi} = \frac{4}{\pi}\left(\frac{d}{m}\right)^2 \frac{r_0|F|}{v_c}} \tag{6.25}$$

where g has been replaced by the expression given in Eq. (6.1). Alternatively, it is sometimes more convenient to work with the full width at half maximum (FWHM), and from Eq. (6.21) this is given by

$$\zeta_D^{\text{FWHM}} = \left(\frac{3}{2\sqrt{2}}\right)\zeta_D^{\text{total}} \tag{6.26}$$

For a given material and Bragg reflection the Darwin width ζ_D (Eq. (6.25)) is a constant, independent of the wavelength[4]. The same is not true for the *angular* Darwin width. The expression for the width ζ_D was derived by assuming a perfectly collimated, white incident beam. The other extreme is to consider the reflectivity of a crystal in a perfectly monochromatic beam as the incident angle is varied. It is quite straightforward to do this using the differential form of Bragg's equation:

$$\frac{\Delta\lambda}{\lambda} = \frac{\Delta\theta}{\tan\theta} \tag{6.27}$$

It follows immediately that the angular Darwin widths are

$$\boxed{w_D^{\text{total}} = \zeta_D^{\text{total}} \tan\theta} \tag{6.28}$$

[4]This is of course neglecting the small energy dependence of the dispersion corrections to the unit cell structure factor.

and

$$w_{\mathrm{D}}^{\mathrm{FWHM}} = \left(\frac{3}{2\sqrt{2}}\right)\zeta_{\mathrm{D}}^{\mathrm{total}} \tan\theta \tag{6.29}$$

The angular Darwin width thus varies with energy through its dependence on $\tan\theta$: as the wavelength is reduced the Bragg angle also becomes smaller, and hence so does the angular Darwin width.

Monochromators at synchrotron beamlines are most commonly fabricated from silicon. The reason is that the semiconductor industry has created a huge demand for defect-free, perfect single crystals, ensuring that the unit cost is low. In addition, silicon can be machined into complex optical elements (focusing monochromators, etc.). It also has the convenient property that the coefficient of thermal expansion passes through zero near the boiling temperature of liquid nitrogen, with the consequence that possible distortions arising from the heat deposited by the intense white beam from a synchrotron can be minimised by cryo-cooling. Silicon is by no means the only choice, and in recent years diamond has become a popular alternative, due to the fact that it has the highest thermal conductivity of any solid, and a low absorption. Both of these factors ensure that any thermal distortions produced by the incident white beam are minimised. In Table 6.1 the Darwin widths $\zeta_{\mathrm{D}}^{\mathrm{FWHM}}$ are listed for diamond, silicon, and germanium. The values have been calculated from Eq. (6.26), but by neglecting the dispersion corrections, f' and f''. The Darwin width is typically of order 100×10^{-6}, or 0.1 mrad for a wavelength 1 Å, and is well matched to the natural opening angle, $(1/\gamma)$, of a synchrotron source as described in Chapter 2.

6.4.2 Extinction depth

As an X-ray beam penetrates into a crystal it becomes weaker as part of it is scattered every time it passes through a plane of atoms. From Eq. (6.15) the incident beam is attenuated by an amount $\mathrm{e}^{-Re(\eta)}$ after passing through a single plane of atoms, where $Re(\eta)$ is the real part of the variable η. After N planes it is attenuated by an amount $\mathrm{e}^{-N\,Re(\eta)}$, and in this way it is possible to define a characteristic length for the attenuation of the incident beam. We define the effective number of reflecting layers, N_{eff}, by

$$\mathrm{e}^{-N_{\mathrm{eff}}\,Re(\eta)} = \mathrm{e}^{-1/2} \tag{6.30}$$

or

$$N_{\mathrm{eff}} = \frac{1}{2Re(\eta)} \tag{6.31}$$

The depth that the beam penetrates into the crystal, the so-called extinction depth, is given by the product of N_{eff} and the lattice plane spacing d. The extinction depth Λ_{ext} is given by

$$\Lambda_{\mathrm{ext}} = N_{\mathrm{eff}}\,d = \frac{d}{2Re(\eta)} \tag{6.32}$$

The value Λ_{ext} is not a constant, but varies across the Darwin reflectivity curve. This can be seen from Eq. (6.16) which is re-written as

$$\eta = g\sqrt{1-x^2}$$

As $x \to \pm1$, $\eta \to 0$ and the extinction depth Λ_{ext} diverges to infinity. This means that for $|x| \geq 1$ the attenuation due to absorption processes, which we have so far neglected, solely determines how far the incident wave penetrates into the crystal. In any calculation of Λ_{ext} it is necessary to specify which

point on the Darwin reflectivity curve it refers to. Here the point $x = 0$ is chosen for which $\eta = g$, and the extinction depth is defined by

$$\boxed{\Lambda_{\rm ext}(x=0) = \frac{d}{2g} = \frac{1}{4}\left(\frac{m}{d}\right)\frac{v_c}{r_0|F|}} \tag{6.33}$$

where $\Lambda_{\rm ext}$ refers to the 1/e reduction of intensity, not amplitude.

The extinction depth defined in Eq. (6.33) is inversely proportional to the modulus of the structure factor $|F|$. For moderate or strong reflections it is much smaller than the absorption length. For example, the (4,0,0) reflection in GaAs has a unit cell structure structure factor of

$$\begin{aligned} F_{\rm GaAs}(4,0,0) &= 4\times[f_{\rm Ga}(4,0,0) + f_{\rm As}(4,0,0)] \\ &= 4\times[f^0_{\rm Ga}(4,0,0) + f'_{\rm Ga} + i\,f''_{\rm Ga} + (f^0_{\rm As}(4,0,0) + f'_{\rm As} + i\,f''_{\rm As})] \\ &= 4\times[25.75 - 1.28 - i\,0.78 + (27.14 - 0.93 - i\,1.00)] \\ &= 154.0 - i\,7.1 \end{aligned}$$

(see Section 5.1.7 on page 159). Here the theoretical values of the dispersion corrections f' and f'' are given at an X-ray wavelength of $\lambda = 1.54056$ Å. The volume of the unit cell is $v_c = 180.7$ Å^3, and the (4,0,0) has a d spacing of 1.41335 Å. Using these values the extinction depth of the (4,0,0) reflection in GaAs is calculated to be 0.74 μm. The absorption depth is given by $\sin\theta/(2\mu)$=7.95 μm, where μ=0.0355 μm^{-1} is the absorption coefficient, and $\theta = 33.02°$ is the Bragg angle. It is evident that for this strong reflection the extinction depth is approximately ten times smaller than the absorption depth. In contrast the (2,0,0) reflection is weak, as it corresponds to the Ga and As atoms scattering out of phase. The structure factor of the (2,0,0) is

$$\begin{aligned} F_{\rm GaAs}(2,0,0) &= 4\times[f_{\rm Ga}(2,0,0) - f_{\rm As}(2,0,0)] \\ &= 4\times[f^0_{\rm Ga}(2,0,0) + f'_{\rm Ga} + i\,f''_{\rm Ga} - (f^0_{\rm As}(2,0,0) + f'_{\rm As} + i\,f''_{\rm As})] \\ &= 4\times[19.69 - 1.28 - i\,0.78 - (21.05 - 0.93 - i\,1.00)] \\ &= -6.96 + i\,0.91 \end{aligned}$$

and the extinction depth is 8.1 μm, more than a factor of two larger than the absorption depth of 3.9 μm.

6.4.3 The integrated intensity

It is also of interest to evaluate the integrated intensity of the Darwin reflectivity curve, and to compare it with the kinematical result given by Eq. (5.31) in Chapter 5. In terms of the variable x, from Eq. (6.21) the area under the Darwin curve shown in Fig. 6.5 is

$$2 + 2\int_1^\infty \left(x - \sqrt{x^2-1}\right)^2 dx = \frac{8}{3}$$

Using Eq. (6.19) this can be converted into an integrated intensity in terms of the variable ζ, with the result that

$$\begin{aligned} I_\zeta &= \frac{8}{3}\frac{g}{m\pi} = \frac{8}{3}\frac{1}{m\pi}\frac{2d^2|F|r_0}{mv_c} \\ &= \frac{8}{3}\frac{1}{m\pi}2\left(\frac{m\lambda}{2\sin\theta}\right)^2\frac{|F|r_0}{mv_c} = \left(\frac{8}{6\pi}\right)\frac{\lambda^2 r_0|F|}{v_c\sin^2\theta} \end{aligned}$$

The kinematical result was derived using the assumptions that the incident beam is monochromatic, and that the intensity is integrated by rotating the crystal through the Laue condition. It is thus necessary to multiply the expression above by a factor of $\tan\theta$ to convert from units of ζ to angle (see Eq. (6.28)). Here it is further assumed that the crystal is large enough that it intercepts the whole beam. The scattered intensity is then proportional to the product of the flux, Φ_0, and cross-sectional area, A_0, of the incident beam. Therefore the integrated intensity recorded by rocking a perfect crystal through the Laue condition is

$$\begin{aligned} I^P_{\rm sc} &= \Phi_0 A_0\, I_\zeta\, \tan\theta \\ &= \Phi_0 A_0 \left(\frac{8}{6\pi}\right)\frac{\lambda^2 r_0|F|}{v_c\sin^2\theta}\tan\theta \\ &= \left(\frac{8}{3\pi}\right)\frac{\Phi_0 A_0\lambda^2 r_0|F|}{v_c\sin 2\theta} \end{aligned}$$

For completeness it is also necessary to allow for the polarization state of the incident beam. As the integrated intensity given by the above is proportional to $|F|$, the appropriate polarization factor assuming an unpolarized beam is $(1+|\cos 2\theta|)/2$. Similarly the Debye-Waller factor is e^{-M}. Altogether the integrated intensity from a perfect crystal scattering in a symmetric Bragg geometry is

$$\boxed{I^P_{\rm sc} = \left(\frac{8}{3\pi}\right)\frac{\Phi_0 A_0\lambda^2 r_0|F|}{v_c\sin 2\theta}\left(\frac{1+|\cos 2\theta|}{2}\right)e^{-M}} \tag{6.34}$$

At first sight is might appear somewhat peculiar that the integrated intensity from a perfect crystal depends on $r_0|F|$, and not $r_0^2|F|^2$ as was the case for kinematical theory. The reason for this is apparent from an inspection of Fig. 6.5, and Eq. (6.25). The central region of the Darwin curve has a reflectivity of 100%, and as the width is proportional to $|F|$, so is the integrated area.

It is instructive to compare the expression for the integrated intensity from a perfect crystal with the corresponding one derived using the kinematical approximation. This comparison has already been discussed qualitatively in Chapter 5. There in the section on extinction (page 182) it was stated that crystals are rarely ideally imperfect as the model of a mosaic crystal requires, and that measured intensities are nearly always smaller than predicted by kinematical theory. One reason for this is that the mosaic blocks have a finite size, and dynamical (or multiple) scattering effects will be present at some level. The reduction of intensities from dynamical effects is known as primary extinction, and here a quantitative comparison is made between the intensities predicted by kinematical and dynamical theory.

We imagine that the reflection from a perfect crystal is measured where the extinction depth is much smaller than that due to absorption. The integrated intensity is then given by Eq. (6.34). The crystal is

now deformed to produce a mosaic structure. This can be done, for example, by heating it up to just below its melting temperature, and then plastically deforming it[5]. In the limit that the deformed crystal approaches the ideally imperfect mosaic crystal the penetration of the X-ray beam will be determined by absorption. For a mosaic crystal with an extended face the integrated intensity is given by Eq. (5.31) as

$$I_{\rm sc}^{M} = \left(\frac{1}{2\mu}\right)\frac{\Phi_0 A_0 \lambda^3 r_0^2 |F|^2}{v_c^2 \sin 2\theta}\left(\frac{1+\cos^2 2\theta}{2}\right)e^{-2M} \tag{6.35}$$

where μ is the absorption coefficient. The integrated intensity from a mosaic crystal is therefore larger than that from a perfect one by a factor of

$$\frac{I_{\rm sc}^{M}}{I_{\rm sc}^{P}} = \left(\frac{3\pi}{16}\right)\frac{\lambda r_0 |F|}{\mu v_c} \tag{6.36}$$

For clarity the polarization and Debye-Waller factors have been neglected.

To take a definite example, we consider again the (4,0,0) reflection from GaAs. With the values of the parameters given in the section on the extinction depth above the ratio of integrated intensities is $I_{\rm sc}^{M}/I_{\rm sc}^{P} \approx 6$. This illustrates the fact that in general the integrated intensity from a mosaic crystal exceeds that from a perfect crystal, by a factor that is proportional to $|F|$. This presents the problem that when performing a crystallographic study to determine the structure of a material, it has to be determined whether it is appropriate to use kinematical or dynamical scattering theory. In practice most crystals are neither completely perfect nor ideally imperfect, but yield integrated intensities somewhere between the values predicted by the two theories. Data from crystallographic studies are nearly always analyzed using the kinematical approximation, and then corrections to the data are made for extinction effects. (The reader is referred to the International Tables of Crystallography for a thorough discussion of applying extinction corrections.) To complete this discussion we also calculate the intensity ratio for the (2,0,0) reflection from GaAs. With the parameters given above the intensity ratio is $I_{\rm sc}^{M}/I_{\rm sc}^{P} \approx 0.2$. Somewhat surprising in this case of a very weak Bragg reflection the kinematical theory appears to predict a smaller intensity than the dynamical one. The reason is that so far absorption effects have been neglected in the dynamical theory. Once these are included it can be shown that in the limit of weak scattering (small $|F|$) the dynamical and kinematical theories yield the same result. Absorption effects are considered further in Section 6.4.6.

6.4.4 Standing waves

The total wavefield above a crystal is composed of the incident T wave, proportional to $\mathrm{e}^{i\mathrm{k}_y y}\mathrm{e}^{i\mathrm{k}_z z}$, and the diffracted S wave, proportional to $\mathrm{e}^{i\mathrm{k}_y y}\mathrm{e}^{-i\mathrm{k}_z z}$ as depicted in Fig. 6.4. Here the y-axis points to the right along the surface of the crystal, and the z-axis points vertically down. At $z = 0$ the two waves have amplitudes T_0 and S_0 in the complex ratio r as given by Eq. (6.20). Thus *above* the surface, $z < 0$, the total wave amplitude is

$$A_{total} = T_0\,\mathrm{e}^{i\mathrm{k}_y y}\left[e^{i\mathrm{k}_z z} + re^{-i\mathrm{k}_z z}\right]$$

In general $r = |r|\mathrm{e}^{i\phi}$, where both the modulus $|r|$ and phase ϕ depend on the variable $x = \epsilon/g$, as plotted in Fig. 6.5 and 6.6. The intensity $I(z, x)$ normalised to T_0=1 above the crystal surface follows as

$$\begin{aligned} I(z,x) = |A_{total}|^2 &= \left[\mathrm{e}^{i\mathrm{k}_z z} + |r|\mathrm{e}^{i\phi}\mathrm{e}^{-i\mathrm{k}_z z}\right]\left[\mathrm{e}^{-i\mathrm{k}_z z} + |r|\mathrm{e}^{-i\phi}\mathrm{e}^{i\mathrm{k}_z z}\right] \\ &= 1 + |r|^2 + |r|\mathrm{e}^{i\phi}\mathrm{e}^{-i2\mathrm{k}_z z} + |r|\mathrm{e}^{-i\phi}\mathrm{e}^{i2\mathrm{k}_z z} \end{aligned}$$

[5] Amongst other things this technique is used to produce monochromator crystals for neutron scattering instruments. Single crystal wafers of nearly perfect Ge are repeatedly deformed to produce a mosaic width of approximately 0.25°.

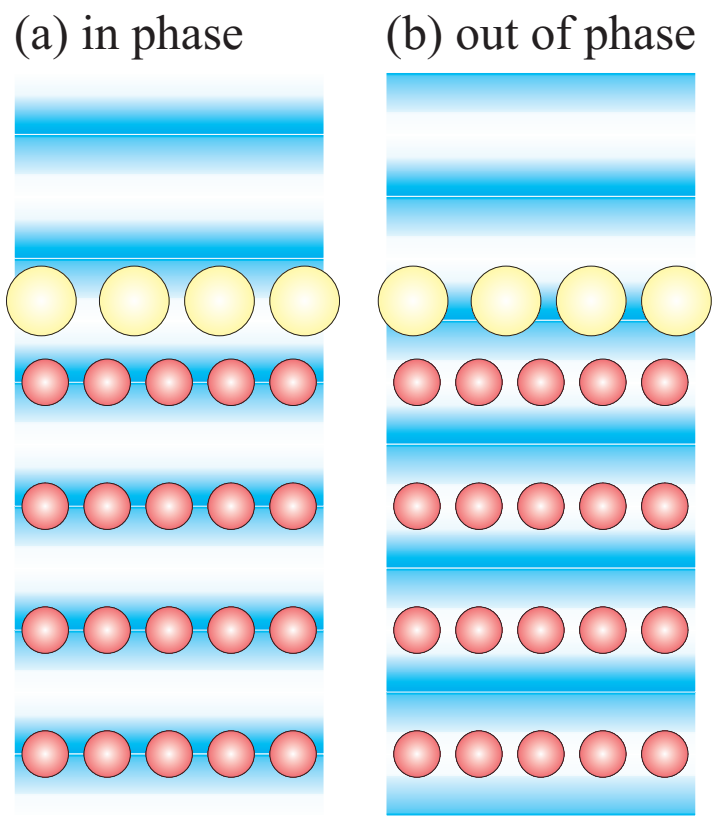

Fig. 6.7 The standing wavefield changes phase with respect to the lattice planes throughout the region of total reflectivity. (a) On one side ($x = 1$, Fig. 6.5) the standing wave has nodes between the lattice planes, and on the other side (b) ($x = -1$) at the lattice planes. The standing wavefield extends beyond the crystal surface, and the height of an absorbed layer (represented by larger circles) can be determined by their fluorescent yield vs the phase of the standing wave.

Here the reader should note that z is a spatial variable with dimension of length, while $x = \epsilon/g$ is the dimensionless independent variable we introduced to describe the Darwin reflectivity curve. Since the modulus of the wavevector transfer for the geometry considered is given by $Q=2k_z$, the above equation for $I(z, x)$ simplifies to become

$$I(z, x) = 1 + |r|^2 + 2|r|\cos(\phi - Qz) \tag{6.37}$$

This equation describes the standing wave intensity above the surface of a crystal. For $x = 1$ the incident and diffracted waves are in phase ($\phi = 0$), and $I(z, x = 1)= 2(1 + \cos(Qz))$. For $x = -1$, the two wavefields are out of phase ($\phi = -\pi$), and $I(z, x = -1)= 2(1 - \cos(Qz))$. Thus as a function of Qz the standing wave intensities at $x = -1$ and $x = 1$ oscillate in quadrature. The standing wave intensity for $x = 1$ is a maximum when $Qz = 2p\pi$, p integer, *i.e.* when $z = pd$, whereas for $x = -1$ the intensity is a maximum when $z = (p + 1)d/2$. The wavefield inside the crystal is also a standing wave, but with an amplitude decaying with the penetration depth.

The existence of standing waves has some interesting consequences:

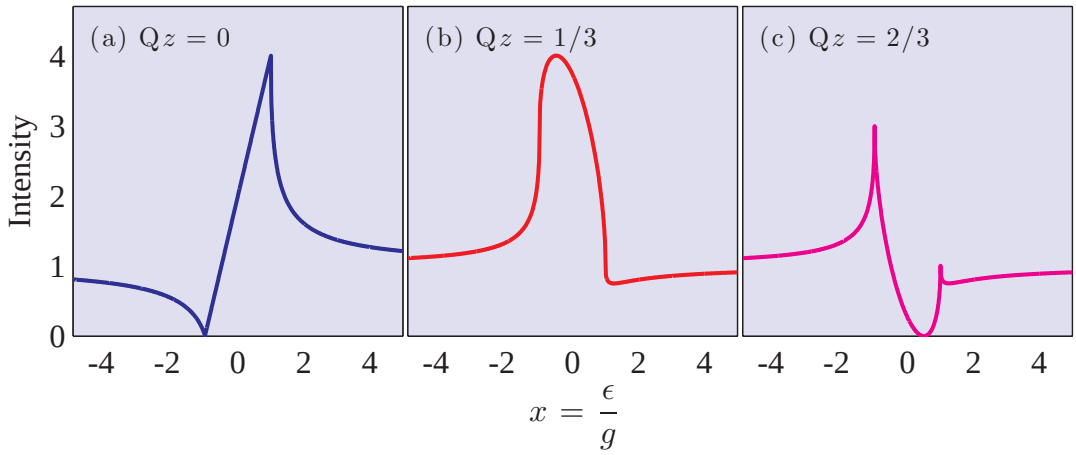

Fig. 6.8 Illustration of the sensitivity of the intensity of X-ray standing waves to Qz. The solid lines have been calculated from Eq. (6.37) using the phase ϕ and the modulus of the amplitude reflectivity $|r|$ obtained from Eq. (6.20).

(a) For the in-phase point the intensity is maximal at the atomic planes, *i.e.* where the density of absorbing electrons is high. For the out-of-phase point the opposite is true. Therefore the influence of absorption is more pronounced when the X-ray wavefields are in phase than when they are out of phase. When absorption is neglected the Darwin curve (Fig. 6.5) is symmetric, but this symmetry will be broken when absorption is taken into account – the right hand side of the curve will be more attenuated than the left hand side, *i.e.* the resulting reflectivity curve becomes progressively more depressed at higher scattering vectors.

(b) The standing wavefield continues of course outside the crystal as shown schematically in Fig. 6.7. As x is scanned through the Laue condition the maximum of $I(z, x)$ above the crystal moves by half a lattice spacing. It follows that if a layer of atoms different to those in the bulk crystal is absorbed on its surface then the atoms in the over layer will fluoresce as the maximum of $I(z, x)$ sweeps through them. To a first approximation it might reasonably be assumed that the fluorescent yield is proportional to $I(z, x)$. In Fig. 6.8 we plot $I(z, x)$ (Eq. (6.37)) for various values of Qz, from which it should be apparent that the fluorescent yield will depend sensitively on the distance z of the over layer above the crystal. In this way X-ray standing waves provide a sensitive method for measuring the spacing of layers deposited on perfect crystals [Batterman, 1964, Andersen et al., 1976].

6.4.5 Higher-order reflections

It has been shown in Section 6.2 that the centre of the Darwin reflectivity curve is offset from the reciprocal lattice points G $= m2\pi/d$ by an amount proportional to $1/m$ (Eq. (6.7)). While in Section 6.4.1 it was shown that the Darwin width varies faster than $1/m^2$ (Eq. (6.25)), since $|F|$ decreases with increasing m due to the reduction of the atomic form factor with increasing Q. This is illustrated in Fig. 6.9.

The variation of $\zeta_{\rm D}$ and the displacement ζ_0 with m has some important implications when considering higher-order reflections from a monochromator crystal. According to Bragg's law a crystal illuminated by a collimated but white beam will not only reflect the desired wavelength $\lambda = 2d \sin\theta$,

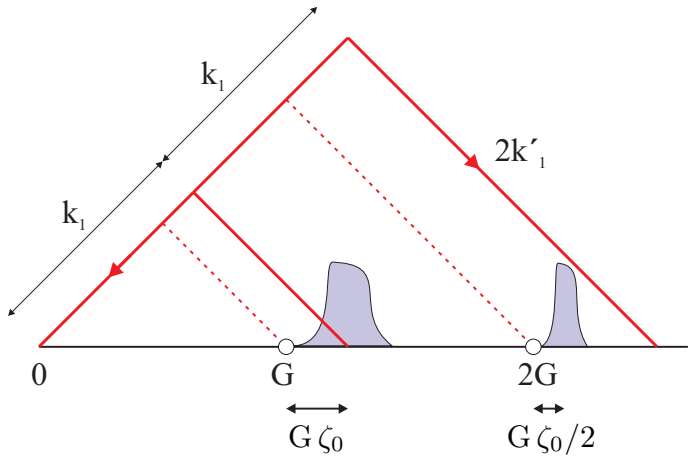

Fig. 6.9 The reciprocal lattice of a stack of atomic planes separated by a distance d is a line of points at positions given by $m\mathrm{G} = m2\pi/d$, where m is an integer. The centres of the Darwin reflectivity curves are offset from these points by an amount $\mathrm{G}\zeta_0$, varying with m as $1/m$, whereas the Darwin width ζ_D varies faster than $1/m^2$. (Note: the scale has been exaggerated.) The crystal is set to reflect a central wavelength of $\lambda_1 = 2\pi/\mathrm{k}_1$. If the incident spectrum also contains $\lambda_1/2 \equiv 2\mathrm{k}_1$, then the different dependences of ζ_D and $\mathrm{G}\zeta_0$ on m ensures that the reflectivity from this component is small.

but also all multiples of λ/m. When performing experiments this can be a major source of irritation, and it is often necessary to take steps to reduce the higher-order contamination[6]. For perfect crystals the situation is not as bad as it may first appear, as illustrated in Fig. 6.9. The different dependences of ζ_D and ζ_0 with the reflection order m ensure that the contribution from the higher-order components is suppressed. One way to increase the suppression of higher-order contamination is to use a double crystal monochromator. Offsetting the angle of the second crystal by a small amount of order $g_0/(2\pi)$ will further reduce the reflectivity of the higher-order components without affecting significantly that of the fundamental wavelength.

From Eqs. (6.7) and (6.25) the explicit relationship between the refractive offset and the Darwin width is

$$\zeta^{\mathrm{offset}} = \frac{\zeta_0}{m} = \frac{\zeta_\mathrm{D}^{\mathrm{total}}}{2}\frac{|F_0|}{|F|} \tag{6.38}$$

It follows that the angular offset $\Delta\theta$ in degrees is

$$\Delta\theta = \frac{\zeta_\mathrm{D}^{\mathrm{total}}}{2}\frac{|F_0|}{|F|}\tan\theta\,\frac{360^\circ}{2\pi} \tag{6.39}$$

For example, the Si (111) reflection with $\lambda = 1.54056$ Å has a Darwin width of $w_\mathrm{D}^{\mathrm{total}} = 0.0020^\circ$ (see Eq. (6.29)), and a refractive offset of 0.0018°. An alternative expression for the offset $\Delta\theta$ in terms of δ, the difference of the refractive index from 1 (Eq. (3.1)), is

$$\Delta\theta = \frac{2\delta}{\sin 2\theta}\,\frac{360^\circ}{2\pi} \tag{6.40}$$

which can be shown to be equivalent to Eq. (6.39).

[6] This can include the use of X-ray mirrors as explored in Chapter 3.

6.4.6 Effect of absorption

For a real crystal absorption has to be included in any calculation of the Darwin reflectivity curve. The way that this is achieved can be understood from a consideration of Fig. 6.2. If absorption is non negligible, then the transmitted wave not only undergoes a change in phase, proportional to g_0, but it is also attenuated. Thus absorption effects can be included by allowing g_0 to become complex, where the imaginary part of g_0 is proportional to the absorption cross-section. Similar considerations apply to the reflected wave. Equations (6.1) and (6.2) are therefore replaced by

$$g_0 = \left(\frac{2d^2 r_0}{m v_c}\right) F_0 \tag{6.41}$$

with

$$F_0 = \sum_j (Z_j + f'_j + i f''_j) \tag{6.42}$$

and

$$g = \left(\frac{2d^2 r_0}{m v_c}\right) F \tag{6.43}$$

with

$$F = \sum_j (f_j^0(\mathbf{Q}) + f'_j + i f''_j) \mathrm{e}^{i\mathbf{Q}\cdot\mathbf{r}_j} \tag{6.44}$$

where f'_j and f''_j are the real and imaginary parts of the dispersion correction to the atomic scattering length $f^0(\mathbf{Q})$, and j labels the atoms in the unit cell.

With these alterations the formulae for the reflectivity are essentially the same, except that the variable x in Eq. (6.19) is now a complex number, x_c, which is given by

$$x_c = m\pi \frac{\zeta}{g} - \frac{g_0}{g} \tag{6.45}$$

with g_0 and g complex. To calculate the reflectivity curves for a given value of ζ one can plot the result *versus* the real part of x_c, so that the amplitude reflectivity may be written as

$$r(Re(x_c)) = \left(\frac{S_0}{T_0}\right) = \begin{cases} \dfrac{1}{x_c + \sqrt{x_c^2 - 1}} = x_c - \sqrt{x_c^2 - 1} & \text{for } Re(x_c) \geq 1 \\ \dfrac{1}{x_c + i\sqrt{1 - x_c^2}} = x_c - i\sqrt{1 - x_c^2} & \text{for } |Re(x_c)| \leq 1 \\ \dfrac{1}{x_c - \sqrt{x_c^2 - 1}} = x_c + \sqrt{x_c^2 - 1} & \text{for } Re(x_c) \leq -1 \end{cases}$$

and as usual the intensity reflectivity is obtained by taking the absolute square of $r(Re(x_c))$.

The effects of absorption on the Darwin reflectivity curve are illustrated in Fig. 6.10(a)⋆, where the specific example of the Si (111) reflection has been taken. As expected the effect of absorption is more pronounced near $x \approx 1$ than at $x \approx -1$, because near $x \approx 1$ the X-ray wavefield is in phase with the position of the atomic planes. As the photon energy is increased the effect of absorption is diminished. In Fig. 6.10(b)⋆ the Darwin curves are plotted *versus* the rotation angle of the crystal in milli degrees at various energies. This part of the figure also serves to illustrate the point that, whereas the relative

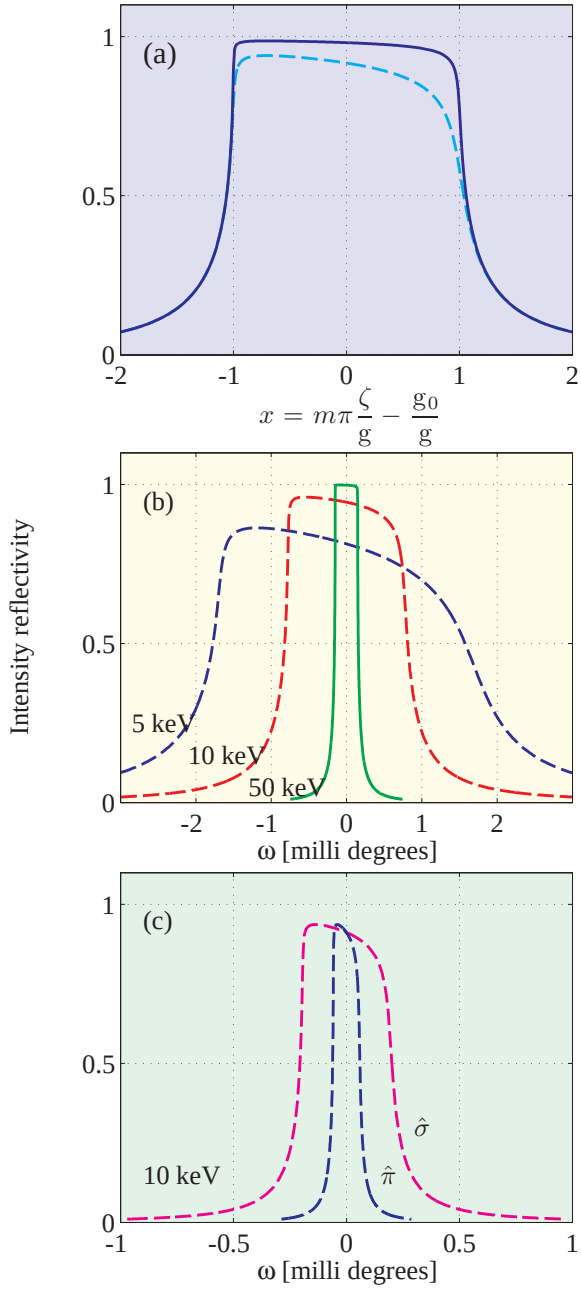

Fig. 6.10 ⋆ Effect of absorption and polarization on the Darwin curve of the Si (*hhh*) reflections. (a) Si (111) plotted as a function of the variable x (see Eq. (6.19)) for $\hat{\sigma}$ polarization. Solid line: λ=0.70926 Å, with $F_0 = 8\times(14+0.082-i\,0.071)$ and $F = 4|1-i|\times(10.54+0.082-i\,0.071)$. Dashed line: λ=1.5405 Å, with $F_0 = 8\times(14+0.25-i\,0.33)$ and $F = 4|1-i|\times(10.54+0.25-i\,0.33)$. (b) Si (111) plotted as a function of the rotation angle of the crystal in milli degrees (see Eq. (6.28)) at various energies for $\hat{\sigma}$ polarization. (c) Si (333) plotted with either $\hat{\sigma}$ (magenta) or $\hat{\pi}$ (blue) polarization.

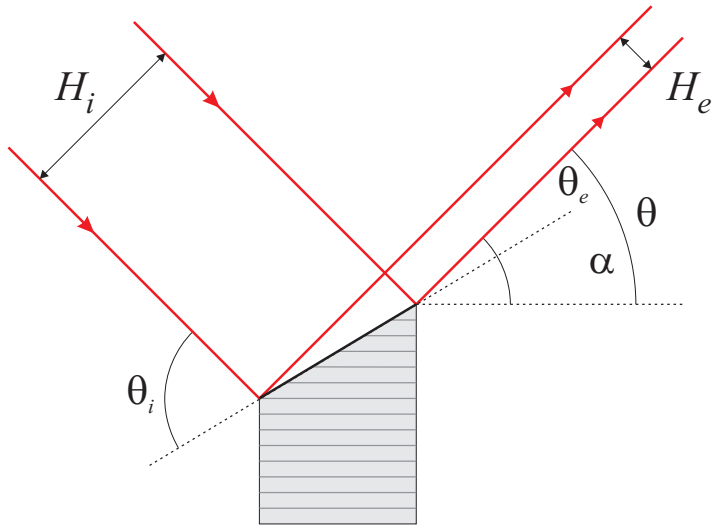

Fig. 6.11 Asymmetric Bragg reflection. The surface of the crystal is at an angle α with respect to the reflecting atomic planes. The widths of the incident and scattered beams are then different. In this case the parameter b is greater than one.

bandwidth ζ (which is proportional to x from Eq. (6.45)) is independent of energy, the angular Darwin width is not.

In Fig. 6.10(c) we provide an example of how the Darwin width depends on the polarization of the incident beam. Up until now we have mostly assumed that the incident beam is polarized perpendicular to the scattering plane, so-called $\hat{\sigma}$ polarization, see Fig. 2.5, for which the polarization factor $P = 1$. With the polarization in the scattering plane – $\hat{\pi}$ polarization – the scattering amplitude is reduced by a factor of $\cos(2\theta)$. In this latter case the primary beam therefore penetrates more deeply into the crystal producing a narrower Darwin width, as evidenced in Fig. 6.10(c). Another way of describing the polarization dependence of the reflectivity curve is to say that in the tails of the Darwin curve perfect crystals are birefringent, *i.e.* they exhibit a difference in the refractive index for waves polarized in orthogonal directions. This birefringence allows the construction of X-ray phase plates for manipulating the polarization of the beam. For example, a quarter-wave plate can be used to convert the polarization from linear to circular.

6.4.7 Asymmetric Bragg geometry

In general the surface of a crystal will not be parallel to the atomic planes which reflect the incident beam, as shown in Fig. 6.11. Let α be the angle between the surface and the reflecting planes. The incident, θ_i, and exit, θ_e, glancing angles are then given by $\theta_i = \theta + \alpha$ and $\theta_e = \theta - \alpha$. For a reflection geometry it is required that both θ_e and θ_i are greater than zero, or in other words that α fulfills the condition $0 < |\alpha| < \theta$. In Fig. 6.11 α has been chosen to be greater than zero. This implies a compression of the width of the exit beam. The asymmetry parameter, b, is defined by

$$\mathsf{b} \equiv \frac{\sin\theta_i}{\sin\theta_e} = \frac{\sin(\theta+\alpha)}{\sin(\theta-\alpha)} \tag{6.46}$$

Symmetric Bragg diffraction corresponds to setting $b = 1$. For the particular case shown in the Fig. 6.11, $b > 1$. The widths of the incident, H_i, and exit, H_e, beams are related by the equation

$$H_i = b\, H_e$$

It turns out that a compression in the width of the exit beam implies an increase in its angular divergence. This is a consequence of Liouville's theorem[7]. By the same reasoning the acceptance angle of the incident beam must decrease to compensate for the increase in the incident beam width. Let the angular acceptance of the incident beam be $\delta\theta_i$, and the reflected beam divergence be $\delta\theta_e$. We now assert that $\delta\theta_i$ and $\delta\theta_e$ are given in terms of the asymmetry parameter b and the Darwin width ζ_D by the equations

$$\delta\theta_e = \sqrt{b}\,(\zeta_D \tan\theta) \tag{6.47}$$

and

$$\delta\theta_i = \frac{1}{\sqrt{b}}\,(\zeta_D \tan\theta) \tag{6.48}$$

These formulae are certainly correct in the symmetric case with $b = 1$ (see Eq. (6.28)). Moreover, since

$$\delta\theta_i\, H_i = \frac{1}{\sqrt{b}}\,(\zeta_D \tan\theta)\; bH_e = \sqrt{b}\,(\zeta_D \tan\theta)\; H_e = \delta\theta_e\, H_e$$

the product of beam width and divergence is the same for the incident and exit beams, as required by Liouville's theorem.

An interesting application of asymmetric crystals is in the measurement of Darwin reflectivity curves. The angular Darwin width is small, typically of order of ~0.002°, *c.f.* Fig. 6.10. Measurement of the reflectivity curve then requires a detector system that has a much better angular resolution than this value. This follows from the fact that the measured curve is the *convolution* of the Darwin reflectivity curve of the crystal and the angular resolution of the detector, or analyzer, system. So if the angular divergence of the analyzer is much smaller than that of the first crystal, then the measured curve is determined solely by the Darwin reflectivity of the first crystal. One way to achieve high angular resolution in the analyzer is to use an asymmetric crystal. From Eq. (6.47), its angular acceptance can be made arbitrarily small by decreasing the value of b. Double crystal spectrometers with two perfect crystals are discussed further in the next section on DuMond diagrams.

In Fig. 6.12 we show data from a double crystal diffractometer composed of two perfect asymmetric silicon crystals. With two asymmetric crystals there are four possible ways of configuring the diffractometer. The narrowest curve is recorded when the first crystal is arranged with $b<1$, and the second with $b>1$. In this case the diffracted beam from the first crystal has the smallest possible angular divergence, which is matched to the narrow angular acceptance of the second.

6.5 DuMond diagrams

An optical element inserted into an X-ray beam is supposed to modify some property of the beam such as its width, its divergence, or its wavelength band. It is useful to describe the modification of the beam by a transfer function. The transfer function relates the input parameters of the beam upstream from the optical element to the output parameters of the beam after the beam has passed the optical element.

[7] Liouville's theorem states that for beams of particles, here photons, the product of beam width and divergence is a constant.

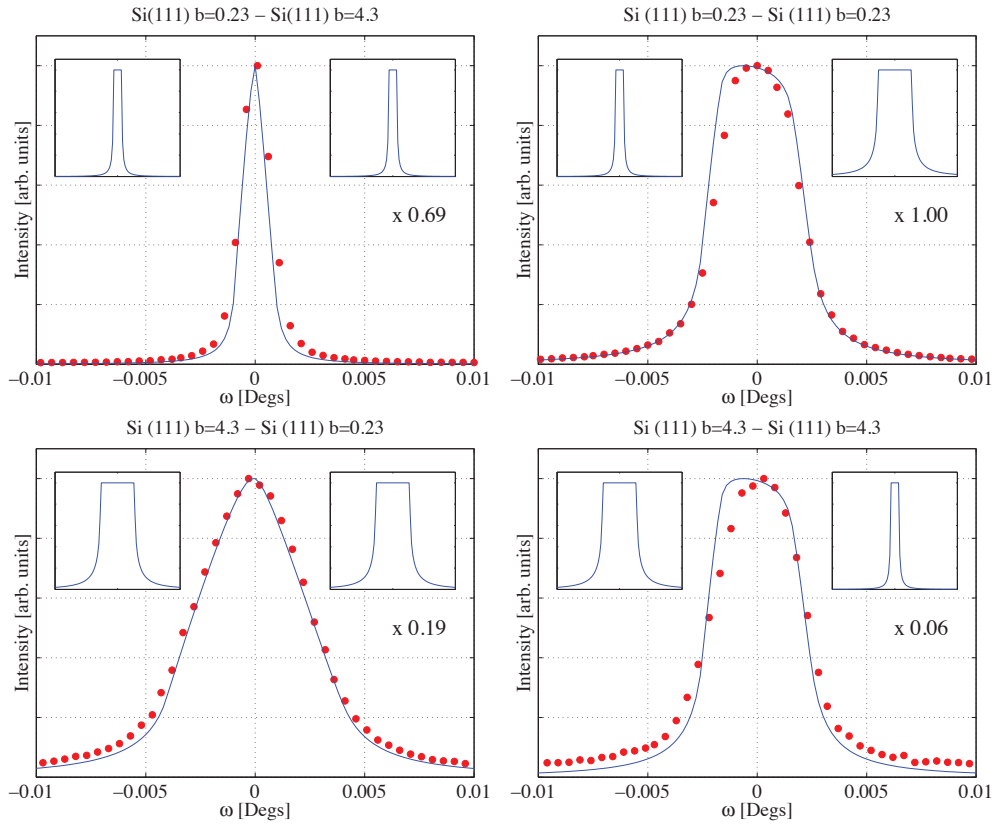

Fig. 6.12 Measured rocking curves for a double crystal diffractometer formed from two asymmetric perfect silicon crystals. The solid lines represent the calculated convolution of two Darwin curves with widths determined by how the asymmetric crystals were configured.

When the optical element is a perfect crystal the relevant beam parameters are amongst other things the beam divergence and the wavelength band. The DuMond diagram is a graphical representation of the transfer function. In the diagram the horizontal axes are the beam divergence, with the input beam to the left and the output beam to the right. The vertical axis is common and is $\lambda/2d$, the wavelength normalized by twice the lattice spacing d. In the crudest approximation, where the finite width of the Darwin curve and refraction effects are neglected, only the points of the incident parameter space in the $(\theta_i, \lambda/2d)$ plane which satisfy $\lambda/2d = \sin\theta_i$ will be reflected. For a white incident beam that falls within an angular window $\theta_{i,\min} < \theta_i < \theta_{i,\max}$ the output side of the DuMond diagram consists of a line given by $\lambda/2d = \sin\theta_e$ with $\theta_{i,\min} < \theta_e < \theta_{i,\max}$.

One crystal

According to Bragg's law, constructive interference of waves scattered from an infinite crystal occurs if the angle of incidence, θ_B, and the wavelength, λ, are related exactly by

$$m\lambda = 2d \sin\theta_B$$

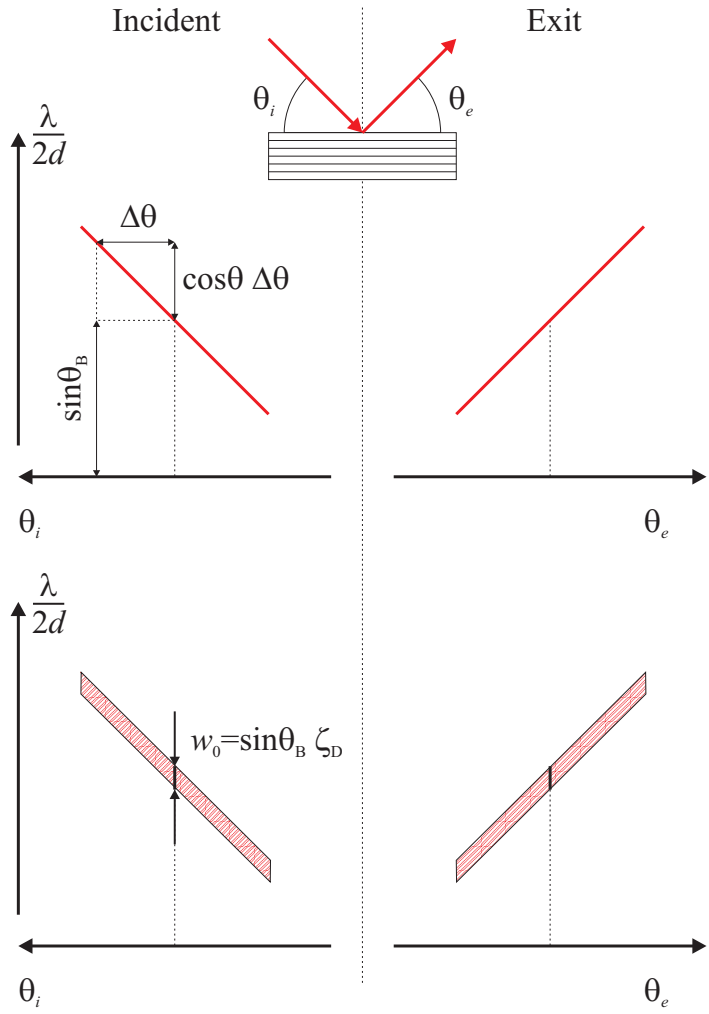

Fig. 6.13 DuMond diagram for symmetric Bragg geometry. In this case the angles of the incident, θ_i, and exit, θ_e, beams relative to the crystal surface are the same. The DuMond diagram is a graphical representation of the Bragg reflection condition, where the axes are angle, relative to the Bragg angle θ_B, and $\lambda/2d$. In (a) the Darwin width has been neglected. The intensity is non-zero for points on the line only. (b) The finite Darwin width broadens the line into a band with a width along the ordinate of $w_0 = \sin\theta_B \zeta_D$.

One way to represent this relationship is to plot a graph with $\lambda/2d$ on the ordinate and θ_B on the abscissa. Any point on the sinusoidal curve gives values of $\lambda/2d$ and θ_B that satisfy Bragg's law. Perfect crystals diffract over a small but finite range in angle and wavelength. When dealing with perfect crystals it is therefore necessary to consider deviations of the incident angle θ_i around θ_B, and deviations of wavelength around the value given by $2d \sin\theta_B$. For asymmetric crystals it is also necessary to consider the exit angle θ_e of the reflected beam.

The DuMond diagram is a graphical way to represent diffraction events, and is composed of two parts: one is a plot of $\lambda/2d$ against $\theta_i - \theta_B$, with θ_i increasing to the left; and the other is a plot of $\lambda/2d$ against $\theta_e - \theta_B$, with θ_e increasing to the right. For small deviations away from the Bragg condition

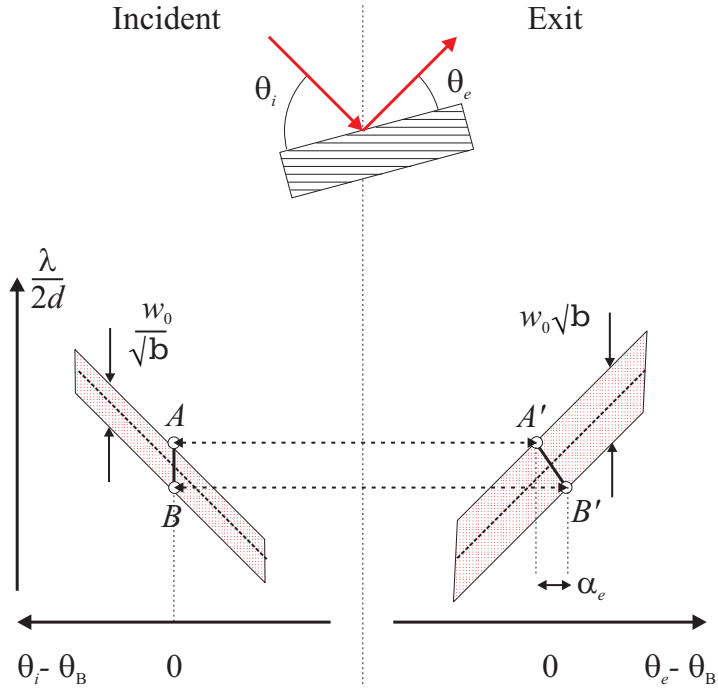

Fig. 6.14 DuMond diagram for asymmetric Bragg geometry. The ratio of the widths of the incident and exit beams is given by the parameter b. This implies that the angular acceptance of the incident beam is reduced by a factor of $1/\sqrt{b}$ while that of the exit beam is increased by the same amount. Thus in the DuMond diagram the incident bandwidth is reduced, and the exit one increased. Points A and B on the incident side are associated with points A' and B' on the exit side. This shows that an incident beam which is parallel and white acquires a finite angular divergence given by α_e when it has been diffracted by a crystal set in asymmetric Bragg geometry.

the sinusoidal dependence of $\lambda/2d$ approximates to a straight line with slope $\cos\theta$. The top part of Fig. 6.13 shows the DuMond diagram for a crystal diffracting according to Bragg's law in a symmetric reflection geometry. When neglecting the finite Darwin width, the reflectivity is non-vanishing only on the line indicated, and the relative change in wavelength $\Delta\lambda/\lambda$ and the deviation $\Delta\theta$ from the Bragg angle are related by

$$\frac{\Delta\lambda}{\lambda} = \frac{\Delta\theta}{\tan\theta}$$

For the symmetric Bragg geometry assumed here the surface coincides with the reflecting planes: the reflection is specular, and the wavelength and exit angle are linked by the same condition as the one above.

The lower part of Fig. 6.13 shows the DuMond diagram for symmetric Bragg geometry, but now including the finite Darwin bandwidth: all wavelengths from a perfectly collimated white source within a relative bandwidth ζ_D have a reflectivity of 100%. Outside of this band, the reflectivity falls off quickly as we move from the dynamical to the kinematical regimes (see Fig. 6.3 and 6.5). In the latter the scattering is located along the crystal truncation rods which run parallel to the surface normal (Section 5.3). In terms of the DuMond ordinate $\lambda/2d$ the width of the central band is

$$w_0 = \frac{\Delta\lambda}{2d} = \left(\frac{\lambda}{2d}\right)\left(\frac{\Delta\lambda}{\lambda}\right) = \left(\frac{\lambda}{2d}\right)\zeta_D = \sin\theta_B\,\zeta_D \tag{6.49}$$

where $\zeta_D = \Delta\lambda/\lambda$ is the Darwin width given by Eq. (6.25). As indicated, symmetry implies that a perfectly collimated incident beam is reflected to a perfectly collimated exit beam.

This is not the case for an asymmetric crystal, where the surface does not coincide with the reflecting planes, as is shown in Fig. 6.14. The exit beam width is now smaller than that of the incident beam. In Section 6.4.7 it has been shown that this implies that the bandwidth of the incident beam is reduced by a factor of $1/\sqrt{b}$, while the bandwidth of the exit beam is increased by a factor of $\sqrt{b}$. It is important to note that the crystal truncation rod is no longer parallel to the reciprocal lattice vector, since it runs perpendicular to the surface. The consequences of these considerations are illustrated in the lower part of Fig. 6.14. A perfectly collimated incident beam is reflected in the band AB. The scattering is elastic, so the point $A(B)$ is transferred to point $A'(B')$ on the exit part of the DuMond diagram. Since the points A' and B' have different abscissa, displaced by the amount α_e, a perfectly collimated incident beam acquires a finite divergence after Bragg reflection.

In the examples of the symmetric and asymmetric Bragg geometries there is an ambiguity left to resolve. This concerns the question of how to relate points on the DuMond diagram of the incident beam with those of the exit beam. For the asymmetric Bragg case, shown in the lower part Fig. 6.14, the point A on top of the incident band is shown connected to the point A' on top of the exit band. (The line runs at right angles to the $\lambda/2d$ axis since the scattering is elastic.) The reason for this is illustrated in Fig. 6.15, which should be compared with Fig. 6.1. The transition from the dynamical to the kinematical regimes must be continuous. In the kinematical regime the scattering lies along the crystal truncation rods (CTR's). If the incident beam is white and parallel then the crystal reflects a band Δk out of the incident beam. A given wavevector in the incident beam, $\mathbf{k}_1$ say, is scattered to a final wavevector $\mathbf{k}'_1$, with $|\mathbf{k}_1| = |\mathbf{k}'_1|$. The direction of $\mathbf{k}'_1$ is found from where the Ewald sphere, indicated by the circular arc, crosses the CTR. For the asymmetric Bragg case the truncation rod does not lie along the direction of the wavevector transfer; it runs perpendicular to the physical surface. From Fig. 6.15(b) this implies that the scattering angle of the exit beam must increase as $|\mathbf{k}'|$ increases. This is consistent with the choice of associating B with B'. Continuity between the dynamical and kinematical regime also implies that the central band of the former does not lie along the wavevector transfer. In other words the reflection is not specular.

The same construction is shown for symmetric Laue geometry in Fig. 6.15(c). From this it is clear that a crystal diffracting in symmetric Laue geometry will impart a finite angular divergence to a parallel, white incident beam.

Two crystals in symmetric Bragg geometry

In Fig. 6.16 a white beam is incident on a crystal at a certain Bragg angle. To simplify the discussion it is assumed, as in the previous section, that the Darwin reflectivity curve may be approximated by a box function. The beam incident on the first crystal is thus the vertical, light shaded band with an angular width $2\Delta\theta_{in}$ in the DuMond diagrams in the lower part of the figure. A second crystal is set to reflect the central ray. This can be done in two ways.

If the Bragg planes in the second crystal are parallel to those in the first crystal, a ray deviating (dotted line) from the central ray by $\Delta\theta_{in}$ will be reflected at the same setting as the central ray. In a DuMond diagram this means that the response band of the second crystal is parallel to that of the first crystal. In scanning the angle of the second crystal there is no overlap with the intensity provided by the first crystal for any of the four settings shown. Only when the angular setting of the second crystal is in between those labelled 2 and 3 will there be scattered intensity after the second crystal. Since the bands are assumed to be box-like, the intensity *versus* angle will be triangular with a FWHM equal to the angular Darwin width w_1 of one crystal, independent of the incident angular bandwidth.

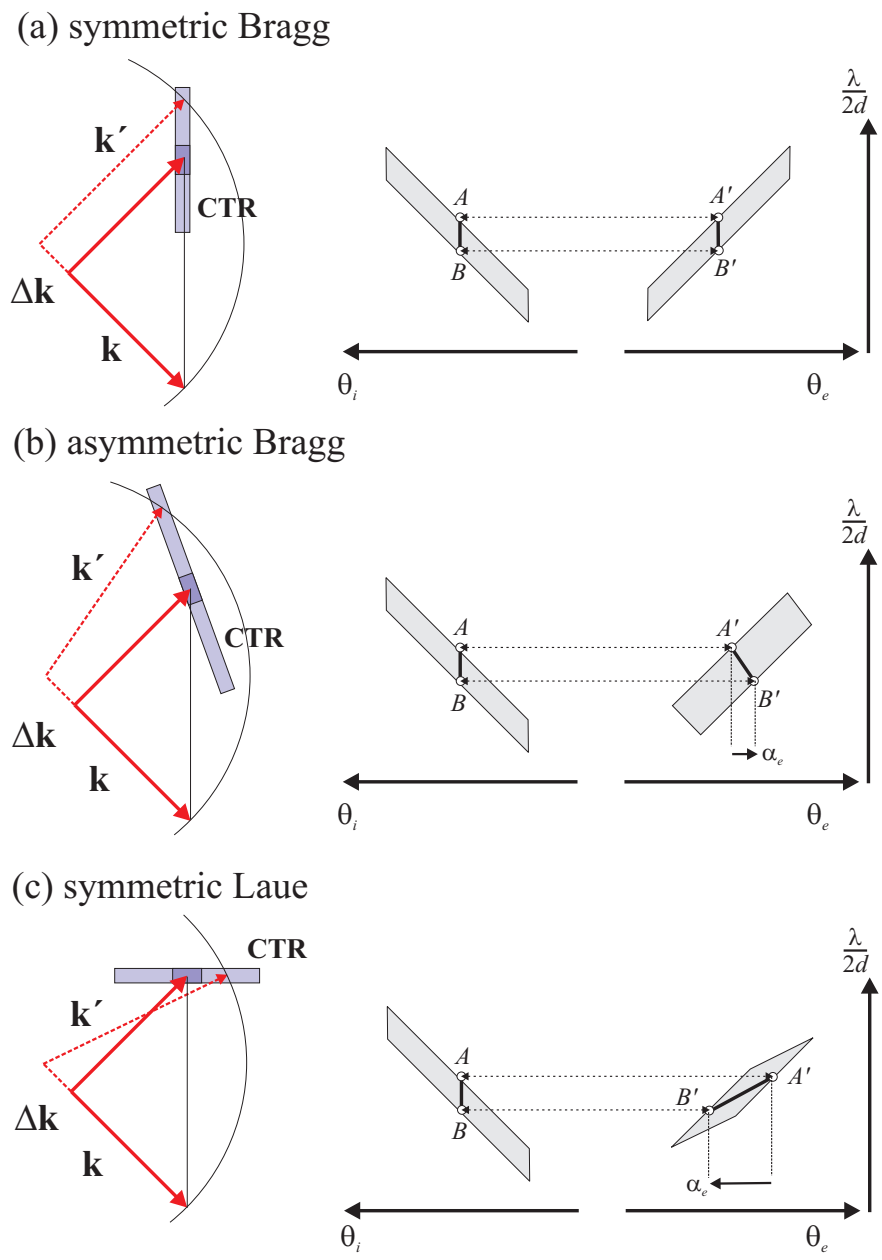

Fig. 6.15 Scattering triangles (left) and DuMond diagrams (right) for (a) symmetric Bragg, (b) asymmetric Bragg and (c) symmetric Laue geometries. In the scattering triangles the crystal truncation rod (CTR) is represented by the rectangular box, with the darker shaded part being the central dynamical band. Continuity between the kinematical and dynamical regimes allows points A, B and A', B' in the DuMond diagrams of the incident and exit beams to be associated with each other in an unambiguous way.

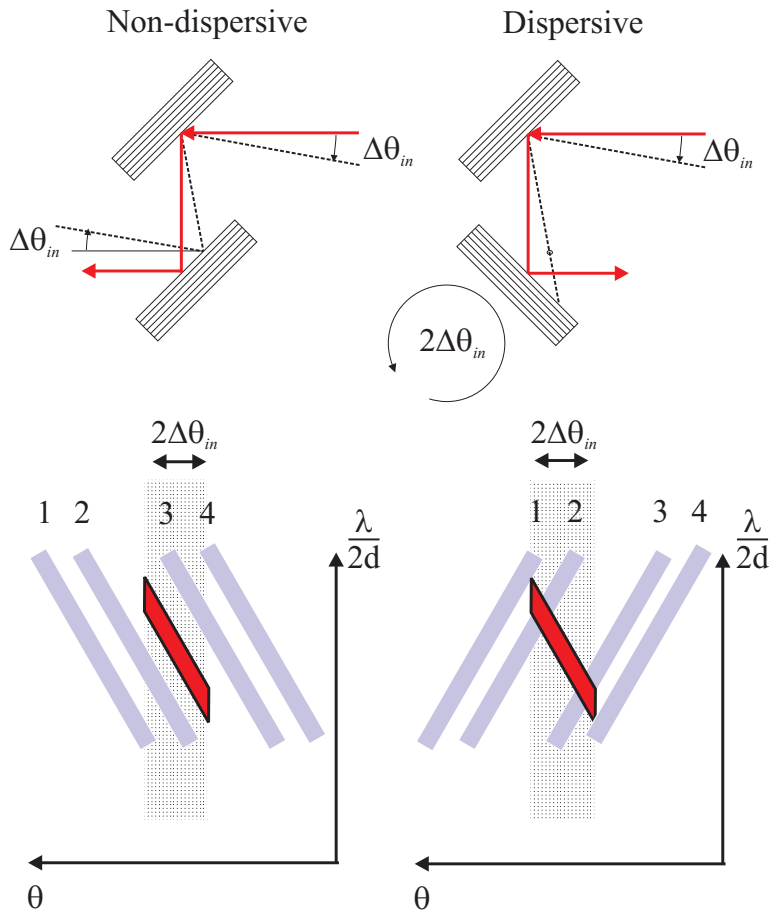

Fig. 6.16 Non-dispersive geometry (left): X-rays from a white source are incident on two crystals aligned in the same orientation. The central ray (full line) will be Bragg reflected by both crystals and will emerge parallel to the original ray. A ray incident at a higher angle than that of the central ray will only be Bragg reflected if it has a longer wavelength. The angle of incidence this ray makes with the second crystal is the same as that it made with the first, and will be Bragg reflected. The DuMond diagram in the lower part shows that a scan of the second crystal has a width equal to the convolution of the Darwin widths of the two crystals, independent of the incident angular divergence. Dispersive geometry (right): A ray incident at a higher angle than the central ray at the first crystal will be incident at a lower angle at the second crystal. The second crystal must be rotated by the amount $2\Delta\theta_{in}$ for Bragg's law to be fulfilled. The geometry is therefore wavelength dispersive.

Furthermore, the reflected wavelength band from the second crystal equals that after the first crystal and is determined by the angular spread $2\Delta\theta_{in}$. This orientation is therefore termed non-dispersive.

On the other hand, in the alternative orientation, the response band of the second crystal has the opposite slope to that of the first crystal. The angular width is now dependent of the incident width – in the limit of a very small Darwin width w_1 it is actually equal to that of the incident width. In the DuMond diagram there will be scattering after the second crystal in all of the positions 2 through 4. The wavelength bandwidth after the second crystal in position 3 is now much smaller than the wavelength bandwidth after the first crystal, and the orientation is termed dispersive. It is clear that this qualitative discussion of the dispersive setting can be sharpened to a quantitative estimate of both the angular and

wavelength bandwidths after scattering from the second crystal.

6.6 Further reading

X-ray diffraction, B.E. Warren (Dover Publications, 1990) Chapter 14.

The optical principles of the diffraction of X-rays, R.W. James (Ox Bow Press) Chapter 2.

Dynamical theory of X-ray diffraction, A. Authier (Oxford University Press, 2001).

X-ray monochromators, T. Matsushita and H. Hashizume, in Handbook of Synchrotron Radiation, Vol. 1b, Ed. E.E. Koch (North holland, 1983) p.261.

6.7 Exercises

6.1 Consider a thick Si crystal where the normal to the surface is in the (100) direction.

(a) What are the Miller indices in symmetric Bragg geometry of the reflection with the lowest Bragg angle?
(b) What is the reflectivity per atomic layer of that reflection?
(c) At a wavelength of 1.54 Å how far should one offset the rotation angle of the sample from the Bragg angle before the reflectivity is reduced by a factor of 100?

6.2 From Eq. (6.20) show that the phase of r is equal to $-\pi$ for $x \leq -1$; $-\text{acos}(x)$ for $|x| \leq 1$, and 0 for $x \geq 1$.

6.3 Prove Eq. (6.26).

6.4 Explain why Eq. (6.33) for the extinction depth refers to the 1/e reduction of intensity rather than amplitude.

6.5 Prove Eq. (6.40).

6.6 Phonons energies are typically in the range 0−100 meV. Inelastic X-ray scattering offers the possibility of measuring phonon dispersion curves. However, as X-ray energies are of order 10 keV, this requires devising a spectrometer with very high energy resolution to detect the relatively small change in photon energy when it creates (or destroys) a phonon.

(a) Starting from Bragg's law, derive a general expression for the resolution $\Delta\mathcal{E}/\mathcal{E}$ in terms of the Bragg angle θ. Under what conditions is the maximum resolution obtained?
(b) Calculate the energy required to achieve the best resolution for a Si (12,12,12) monochromator.
(c) By calculating the Darwin width at the appropriate energy calculate the resolution provided by a Si(12,12,12) monochromator.

6.7 Estimate the extinction depths of the (111) reflections from diamond, silicon and germanium by neglecting the Q and energy dependences of the atomic form factors.

6.8 Consider the (200) reflection from GaAs at 12.4 keV. Compare the extinction depth to the absorption depth. Discuss whether the integrated intensity in a rocking scan is proportional to $|F|$ or to $|F|^2$.

6.9 Evaluate and compare the ratio of widths of the (111) and (333) reflections shown in Fig. 6.10(b) and (c).

6.10 Consider the experimental arrangement in which a white beam is monochromated by a perfect crystal in symmetric Bragg geometry with a Bragg angle of 30°. The monochromatic beam then impinges on a second, asymmetrically cut perfect crystal in which the lattice planes are at an angle of 15° with respect to the surface. The angle of incidence of the beam on the second crystal required to diffract the second beam is either (a) 15° or (b) 45° depending on its orientation. For the two cases make sketches of the expected variation of intensity of beam diffracted by the second crystal as its angle is rotated through the Bragg condition. (You may assume for simplicity that the Darwin curve may be represented by a top-hat function and ignore refraction effects.)